Int Journ Earth Sciences (1999) 88:236–252

ORIGINAL PAPER

L. Hecht · K. Thuro · R. Plinninger · M. Cuney

Mineralogical and geochemical characteristics of hydrothermal alteration and episyenitization in the Königshain granites, northern Bohemian Massif, Germany

Received: 9 July 1998 / Accepted: 12 April 1999

Abstract The late-Hercynian granites of Königshain underwent multistage hydrothermal processes. Extensive high-temperature late-magmatic alteration is, for example, indicated by low Zr/Hf and an REE pattern displaying the tetrad effect. Intensive post-magmatic alteration of the granite occurred along brittle structures. At least two main stages of post-magmatic hydrothermal alteration are involved. The first high-temperature stage, which is characterized by albitization and/or quartz leaching (episyenitization), resulted from fluid–rock interaction with late-magmatic fluids that very probably mixed with external low-salinity fluids. Quartz dissolution was triggered by vapour condensation and/or the cooling of these fluids (below 450 °C) along brittle structures. The high porosity resulting from quartz leaching during stage 1 assisted subsequent circulation of low-temperature fluids at stage 2; the latter is characterized by the chloritization and illitization of episyenites. Almost all major and trace elements were enriched or depleted during one of the main alteration stages. However, Zr, Hf, Th, and Ti were immobile during post-magmatic alteration. The significant depletion of LREE and the enrichment of HREE in albitized samples is controlled by the dissolution of monazite and the new formation of HREE-rich polycrase-(Y) or aeschynite-(Y) during post-magmatic stage 1. Negative Ce anomalies of episyenites are associated with illitization and suggest oxidizing conditions during stage 2.

Key words Hydrothermal alteration · Quartz leaching · Albitization · Chloritization · Illitization · Rare earth elements · Element mobility · Metasomatism · Accessory minerals · Hercynian · A-type granites

L. Hecht (✉)
Lehrstuhl für Angewandte Mineralogie und Geochemie, Technische Universität München, D-85747 Garching, Germany
e-mail: lutz.hecht@geo.tum.de,
Fax: +49-89-28913205

K. Thuro · R. Plinninger
Lehrstuhl für Angewandte, Allgemeine und Ingenieurgeologie, Technische Universität München, D-85747 Garching, Germany

Present address:
L. Hecht · M. Cuney
CREGU – UMR 7566 G2R, BP 23, F-54501
Vandoeuvre/Nancy, France

Introduction

From 1995 to 1997 excavation for two roadway tunnels exposed the late-Hercynian Königshain granites for a total length of 3.3 km. In the course of the excavation, several zones of hydrothermally altered granite were discovered. One of the main features of the altered granite is the dissolution of magmatic quartz. Rocks depleted in quartz by hydrothermal fluids are referred to as episyenites as defined by Lacroix (1920). Quartz dissolution (episyenitization) is a well-known type of subsolidus alteration in granites (Cathelineau 1986). Special attention has been given to episyenites in the Hercynian granites of Central and Western Europe which act as hosts for U mineralisation (Leroy 1978; Dill 1985; Cathelineau 1986; Cathelineau 1987; Turpin et al. 1990; Hecht et al. 1991; Scaillet et al. 1996) or Sn-W mineralisation (Cheilletz and Giuliani 1982). Episyenites were also described from other parts of the world in granites of different ages (Charoy and Pollard 1989; Dempsey et al. 1990; Schoch and Scheepers 1990; Petersson and Eliasson 1997). Episyenites are usually porous rocks that weather easily. Therefore, large underground outcrops such as tunnels offer a unique opportunity to study rocks that were not altered by surface weathering.

The aim of this paper is to discuss the mineralogical and chemical changes involved in hydrothermal alteration including the episyenitization of the Königshain granites and to decipher the genesis of multistage hydrothermal processes.

Geological setting

The Hercynian granites at Königshain (NE of Görlitz) were emplaced at the northeastern margin of the Lusatian Granitoid Complex (LGC). The LGC belongs to the Saxothuringian zone of the mid-European Hercynides and is located at the northern margin of the Bohemian massif (Fig. 1a). The LGC, which is bordered by major faults and overthrusts, is distinct from adjacent Hercynian and pre-Hercynian domains and is interpreted as a Cadomian (Pan-African) terrane of yet unknown origin (Kröner et al. 1994). It includes mostly peraluminous granitoids such as monzogranites, syenogranites, granodiorites, and tonalites (Krauss et al. 1992; Kröner et al. 1994). Some Hercynian granites intruded along large deep-seated regional faults such as the Inner Lausitz fault at the NE margin of the LGC (Krauss et al. 1992). The Hercynian granites comprise amphibole-bearing granodiorites and monzogranites (e.g. at Wiesa; Eidam et al. 1995) as well as biotite-dominated monzogranites such as those at Königshain (Fig. 2). The granites were intruded by mafic dykes (lamprophyres) most probably during Permian and also Mesozoic times. The study area was uplifted since the Late Proterozoic (Eidam et al. 1995).

Analytical methods

Major and trace element compositions of whole-rock samples were analysed by ICP-AES and ICP-MS and/or XRF spectroscopy. ICP-AES and ICP-MS spectrometry were carried out at the CRPG, Nancy, France, according to the method of Govindaraju et al. (1976) and Govindaraju and Mevelle (1987). XRF was performed at the Technical University of Munich with a wavelength-dispersive Siemens spectrometer SRS 303 (Siemens, Erlangen, Germany). XRF analyses were carried out on glass discs, each prepared from 1.5 g powdered sample mixed with $Li_2B_4O_7$ flux. Some samples were analysed by both ICP and XRF spectrometry in order to check the accuracy of the methods applied (see samples 18–14.7 and 6–17.4 in Tables 4 and 5). The deviation between the two methods is mostly well below 15% except for some components with concentrations close to the detection limit.

The chemical composition of minerals was determined by means of a Cameca (Paris, France) SX50 electron microprobe at Nancy I University using mineral as well as synthetic standards and 15 kV accelerating voltage with 10-nA beam current. Backscattered electron (BSE) images and semi-quantitative

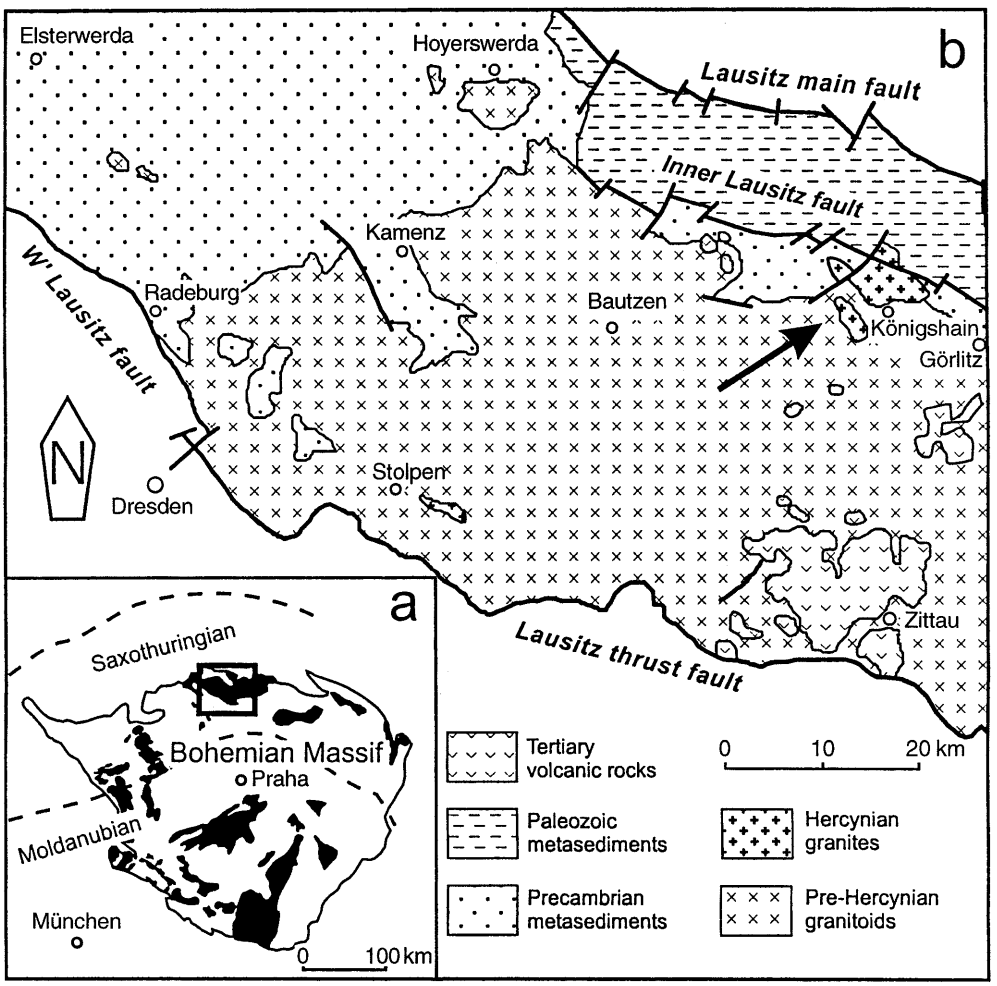

Fig. 1 **a** Location of the study area at the northern border of the Bohemian Massif (granitoids in *black*). **b** Geological environment of the Hercynian granites of Königshain. (According to Krauss et al. 1992; Kröner et al. 1994)

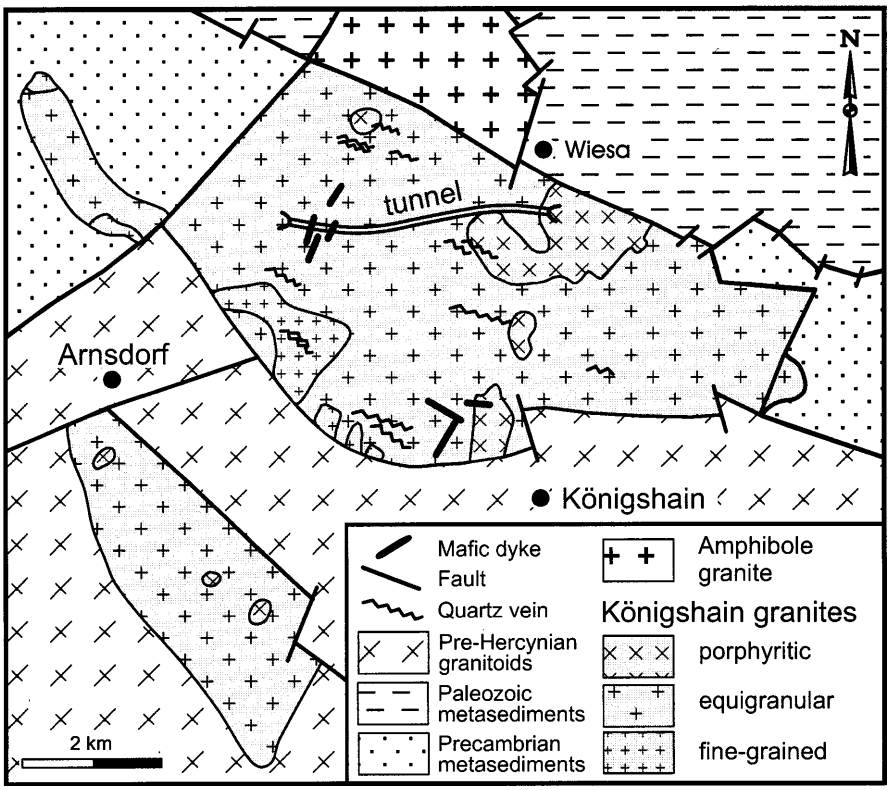

Fig. 2 Sketch map of the Hercynian granites at Königshain. (According to Möbus and Lindert 1967; Eidam and Götze 1991; Eidam et al. 1995; own data)

mineral analysis were performed with a Hitachi (Tokyo, Japan) S2500 Kevex scanning electron microscope (SEM) equipped with an energy-dispersive spectrometer (EDS) at Nancy I University.

Petrography and mineralogy

Königshain granites

The geology and petrography of the Königshain granites were previously studied by Möbus and Lindert (1967) and Eidam and Götze (1991). They distinguished three types of granite: (a) equigranular leucogranite; (b) porphyritic granite; and (c) fine-grained leucogranite. The new highway tunnel offered an excellent cross section through the northern part of the equigranular Königshain granite. Some dykes of fine-grained granite occur within the equigranular granite. The porphyritic type occurs only in the eastern most part of the tunnel (Fig. 2). According to Möbus and Lindert (1967) the granites correspond to biotite–monzogranites with an average biotite content of 8, 2.6 and 1.6 vol.% in the porphyritic, equigranular and fine-grained granites, respectively. The granites are typically of pink-reddish colour. Miarolitic cavities containing molybdenite, wolframite and beryl (Eidam and Götze 1991) are common within the equigranular granite.

Weak subsolidus alteration of the equigranular granite is indicated by the chloritization of some single biotite grains (chlorite 1) and the occurrence of muscovite within feldspars. Primary muscovite could not be identified. For more detailed geological and rock-forming mineral descriptions see Eidam and Götze (1991) and references therein.

Magnetite / ilmenite + fluorite + zircon + pyrite / pyrrhotite + epidote + apatite ± monazite ± anatase are the typical accessory minerals of the Königshain granites according to (Eidam et al. 1995). But Eidam et al. (1995) did not distinguish between the different granite types of Königshain. Except for one sample, all episyenites of this study were formed by the alteration of the equigranular granite. Since accessory minerals are important for the understanding of the behaviour of many trace elements, a detailed study of these minerals was performed in the equigranular granite. Magnetite, fluorite, xenotime, zircon and monazite represent the most important accessory minerals. Magnetite and zircon are mostly euhedral and occur within or close to biotites. Xenotime forms anhedral overgrowth on zircon, but nearly euhedral grains also exist. Fluorite crystallized between or within feldspars. Euhedral to anhedral monazite crystals are common within or close to biotite and magnetite. Very small uraninite grains (<4 μm) are to be found on the crystal margins of monazite. Thorite, which is not very abundant, is enclosed by zircon. Small crystals of a LREE-F-mineral (fluocerite?) and an Mn-bearing Fe–Ti mineral (ilmenite or ilmenorutile?) appear locally, but only within chloritized biotites. Minor accessory minerals composed of Y–Nb (probably fergusonite, $Y(Nb,Ta)O_4$), Y–Si–U and Nb–Si–Th–U are also present within biotite or magnetite. Anatase occurs within chloritized biotite. Apatite is rare and no epidote could be observed.

Episyenites

In the Königshain granites zones of episyenitization are up to several metres thick, following steep-dipping faults which strike approximately 20–30° NNE and 110–130° NW. The episyenites are heterogeneous in composition. Several types of alteration parageneses occur in variable amounts.

The unaltered granite contains typically pink to reddish feldspar. The episyenites show white feldspars due to albitization or sericitization (see below). The episyenites may be hololeucocratic when no chlorite

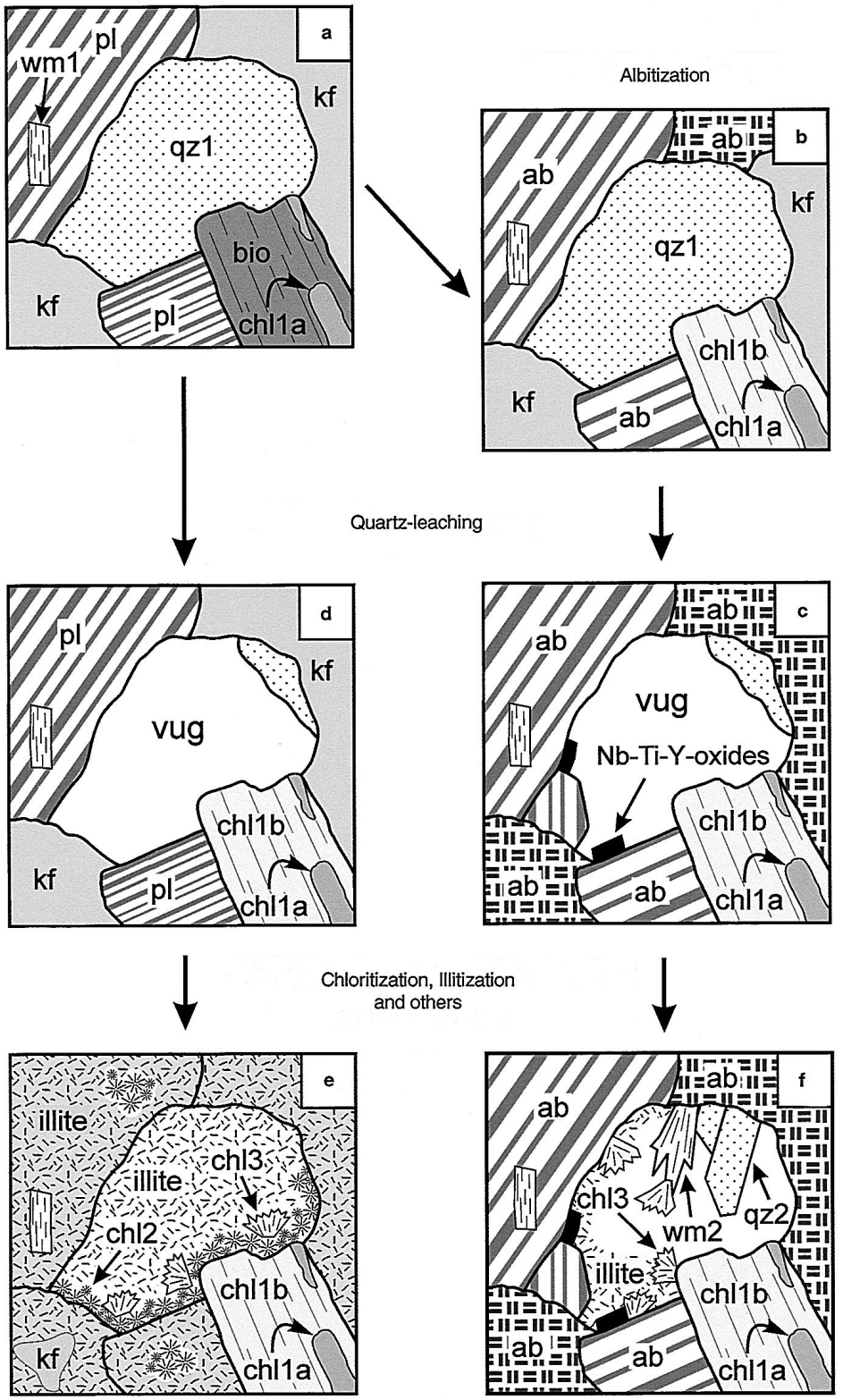

Fig. 3a–f Schematic microtextural sketches of progressive post-magmatic alteration. **a** Equigranular Königshain granite; **b** partial albitization of feldspars before quartz leaching; **c** further albitization of feldspars and leaching of quartz 1 (note the formation of some vug-filling albite and Nb–Y–Ti oxides); **d** quartz leaching without preceding albitization of feldspars; **e** episyenite with intensive illitization ± chloritization of feldspars and vug-filling chlorite and illite (corresponds to sample 97–15); **f** episyenite with albitization and vug-filling quartz, white-mica, chlorite, and illite (synthesis of sample 97–10 and 97–14). *kf* K-feldspar; *pl* plagioclase; *ab* albite; *qz* quartz; *wm* white mica; *bio* biotite; *chl* chlorite

Table 1 Semi-quantitative data for mineral alteration and formation of vug-filling minerals in episyenites

Sample	97–10	97–11	97–12	97–14	97–15[a]	97–23	97–29
Alteration of major components							
Dissolution of quartz	xxx	xxx	xxx	xxx	xxx	xxx	xxx
Albitization of feldspars	xxx			xxx		xxx	
Sericitization of feldspars			xx		xxx		xx
Biotite replaced by:	Chlorite	White mica	Chlorite ± Illite	Chlorite ± Illite	Chlorite ± Illite	White mica	White mica
Vug-filling minerals							
White mica 2 (phengite)		xx				xx	
Chlorite 2			xx		xx		x
Chlorite 3	xx	xx	x	xx	xx	xx	(x)
Illite	x	xx	(x)	xx	xx	(x)	xxx
Pyrite				xx	(x)		xx
Quartz	x	xxx	xxx		(x)	xx	xxx

(x) very minor (rare); *x* minor (weak); *xx* abundant (intermediate); *xxx* very abundant (complete)
[a] Feldspars also replaced by some chlorite

occurs (e.g. 97–23), green spotted with moderate chloritization (e.g. samples 97–10, 97–12), or completely dark green coloured with strong chloritization (e.g. sample 97–15). The magmatic texture of the granite, which is represented mainly by the feldspar framework, is generally preserved; however, brecciation of episyenites, in combination with compaction and/or quartz veining, also occurs. The major mineralogical changes resulting from hydrothermal alteration are illustrated in Fig. 3 and are described herein. Semi-quantitative estimation of the intensity of mineral alteration and the proportion of authigenic minerals are listed for each sample in Table 1. The interpretation of the paragenetic succession during alteration is given in Fig. 4.

Feldspars

K-feldspar and plagioclase can be replaced by albite. Albitized K-feldspar shows the typical chessboard twinning (Slaby 1992). Moderate albitization of feldspars also occurs within the granite outside the episyenite bodies (sample 97–19). Some anhedral to euhedral authigenic albite was observed in vugs of albitized episyenites. Other episyenites show a nearly complete alteration of feldspars to illite and probably other clay minerals. Relics of unaltered K-feldspar in these episyenites indicate that they were not previously albitized.

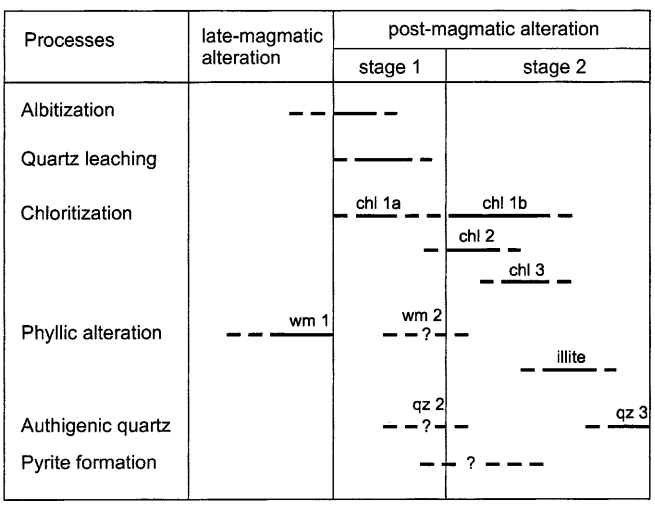

Fig. 4 Paragenetic sequence of alteration events. *wm1* white mica 1; *wm2* white mica 2; *qz2* vug-filling quartz 2; *qz3* vug-filling quartz 3

Quartz

The characteristic feature of episyenites is the absence of magmatic quartz (quartz 1). Newly formed, chiefly idiomorphic quartz may occur in vugs of some episyenites. It has always straight grain boundaries between the individual crystals and rarely shows undulatory extinction. Locally two generations of vug-filling quartz can be distinguished. Quartz 2 crystallized at an early vug-filling stage probably synchronously with white mica 2 (Fig. 4). Quartz 2 is corroded by vug-filling chlorite. Authigenic quartz 3 contains inclusions of vug-filling chlorite and illite and is therefore one of the latest vug-filling minerals in the episyenites.

Chlorite

At least three generations of chlorite can be distinguished within the episyenites. Chlorite 1 is pseudomorphic after biotite and occurs in relatively unaltered granite and in episyenites. Chlorites 2 and 3 occur as vug-filling minerals only within episyenites. Chlorite 2 forms very fine-grained vermicular aggregates or overgrowths in vugs. Coarser-grained tufts of chlorite 3 crystallized after chlorite 2. Both vug-filling chlorite generations are not always developed in the same sample (Table 1). Figure 4 shows the chemical composition of different chlorite generations of the granite and episyenites. Some representative chlorite analyses

Table 2 Chemical composition of chlorites. The structural formula was calculated on the basis of 14 oxygens

Sample	97–7	97–10	97–10	97–15	97–15	97–15	97–10	97–11	97–15
Analysis	8	19	12	1	22	28	30	5	14
Generation	1a	1a	1b	1b	1b	2	3	3	3
SiO_2 wt.%	23.28	23.26	29.45	25.48	26.67	24.62	29.11	29.65	27.13
TiO_2	<0.05	0.07	<0.05	0.07	<0.05	<0.05	<0.05	<0.05	<0.05
Al_2O_3	20.50	20.19	20.99	21.58	19.88	20.07	20.64	23.00	21.45
FeO	42.32	42.02	10.59	30.42	20.23	32.23	10.31	9.15	21.80
MnO	1.32	2.00	<0.20	<0.20	<0.20	<0.20	<0.20	<0.20	<0.20
MgO	1.21	0.74	25.35	12.15	18.51	10.03	24.21	25.83	17.25
CaO	<0.07	0.08	0.08	<0.07	0.10	<0.07	0.12	0.07	<0.07
Na_2O	<0.05	<0.05	<0.05	<0.05	<0.05	<0.05	<0.05	<0.05	<0.05
K_2O	<0.07	0.13	<0.07	<0.07	0.07	<0.07	<0.07	<0.07	<0.07
Total	88.63	88.49	86.46	89.70	85.46	86.95	84.39	87.70	87.63
Si	2.691	2.704	2.888	2.687	2.803	2.717	2.920	2.839	2.787
Al^{IV}	1.309	1.296	1.112	1.313	1.197	1.283	1.080	1.161	1.213
Al^{VI}	1.483	1.469	1.313	1.368	1.264	1.328	1.360	1.435	1.384
Ti	0.000	0.006	0.000	0.006	0.000	0.000	0.000	0.000	0.000
Fe	4.089	4.084	0.868	2.682	1.777	2.974	0.865	0.733	1.873
Mn	0.129	0.197	0.000	0.000	0.009	0.009	0.000	0.000	0.013
Mg	0.208	0.128	3.702	1.908	2.897	1.649	3.618	3.684	2.640
Ca	0.000	0.010	0.008	0.000	0.011	0.000	0.013	0.007	0.000
Na	0.000	0.000	0.000	0.000	0.000	0.000	0.000	0.000	0.000
K	0.000	0.019	0.000	0.000	0.009	0.000	0.000	0.000	0.000
Z	4.000	4.000	4.000	4.000	4.000	4.000	4.000	4.000	4.000
Y	5.909	5.913	5.891	5.964	5.967	5.960	5.856	5.859	5.910
Fe/(Fe+Mg)	0.95	0.97	0.19	0.58	0.38	0.64	0.19	0.17	0.42

are given in Table 2. Chlorite 1 (pseudomorphic after biotite) shows the largest variation in chemical composition. Because of distinct chemical compositions, chlorite 1 was subdivided into chlorite 1a and chlorite 1b (Fig. 5). Chlorite 1a has the highest Fe/(Fe+Mg) which corresponds to that of biotite which was replaced (Table 3). It was most likely to be formed during early post-magmatic alteration (stage 1). Chlorite 1a can be preserved partly during later hydrothermal alteration (stage 2) in episyenites (Fig. 5, analysis 19 of sample 97–10 in Table 2). Chlorite 1b is restricted to episyenites and has significantly lower Fe/(Fe+Mg) than chlorite 1a. Furthermore, chlorite 1b and the vug-filling chlorites 2 and 3 show a large variation in chemical composition which is characterized by decreasing Fe/(Fe+Mg) with increasing Si (Fig. 5). The variation in composition of chlorite 1b in the episyenites reflects presumably different degrees of chemical reequillibration during successive hydrothermal alteration.

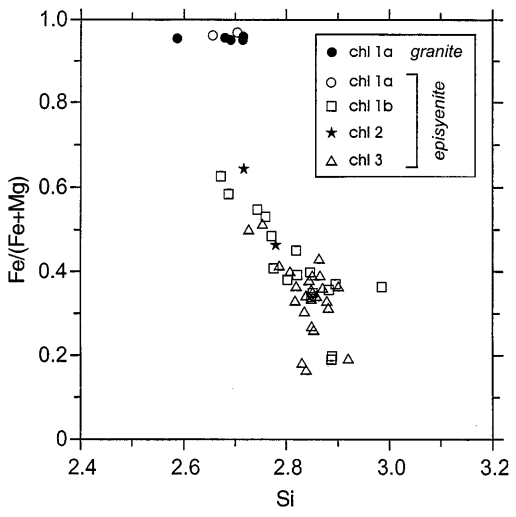

Fig. 5 Chemical composition of chlorite generations 1–3 in equigranular granite and episyenites of the Königshain massif

White mica and illite

White mica 1 (wm1) is assumed to be of late-magmatic origin and was only slightly disturbed by later stages of post-magmatic alteration, including episyenitization. The composition of white mica 1 varies between muscovite and phengite (Table 3). White mica 2 occurs only in episyenites 97–11 and 97–23. It crystallized as radial-shaped tufts in vugs and is phengitic in composition (Table 3). The crystallization of white mica 2 occurred after quartz leaching and preceded the formation of vug-filling chlorites.

Illite occurs as a late vug-filling mineral but also replaces feldspars and chlorite generations 1–3 (Table 3). In some cases the intergrowth of chlorite 3 aggregates with illite suggests that both minerals crystallized at the same time.

Minor and accessory minerals

In the moderately albitized granite (97–19) monazite is partly altered. This fact is indicated by the development of dissolution cavities in the crystal and a new forma-

Table 3 Chemical composition of micas and illites. The structural formula was calculated on the basis of 22 oxygens. *WM 1* white mica 1; *WM 2* white mica 2

Sample	97–19	97–7	97–7	97–7	97–11	97–23	97–15a	97–10	97–11
Analysis	7	3	6	7	1	1	10	9	4
Mineral	Biotite[a]	Biotite	WM 1	WM 1	WM 2	WM 2	Illite	Illite	Illite
SiO_2 wt.%	36.16	36.26	46.75	47.03	48.16	47.00	49.33	52.24	52.56
TiO_2	3.20	1.89	<0.05	<0.05	0.31	0.17	0.09	0.10	<0.05
Al_2O_3	16.85	18.89	33.17	36.27	33.29	31.97	30.47	31.27	30.68
FeO	26.62	26.79	5.18	1.77	3.61	3.60	2.72	1.47	0.87
MnO	0.40	0.82	0.24	<0.20	<0.20	<0.20	<0.20	<0.20	<0.20
MgO	3.79	0.94	0.17	0.00	0.40	0.34	1.81	1.90	2.33
BaO	<0.30	<0.30	<0.30	<0.30	<0.30	<0.30	<0.30	<0.30	<0.30
CaO	<0.07	<0.07	<0.07	<0.07	<0.07	<0.07	<0.07	0.13	0.13
Na_2O	0.17	0.08	0.16	0.37	0.09	0.05	<0.05	0.13	0.09
K_2O	9.55	9.92	11.25	11.14	11.48	10.94	8.08	9.03	10.40
Rb_2O	<0.10	0.18	<0.10	<0.10	<0.10	<0.10	<0.10	<0.10	<0.10
F	0.70	<0.60	<0.60	<0.60	<0.60	<0.60	<0.60	<0.60	<0.60
Cl	0.17	0.11	<0.05	<0.05	<0.05	<0.05	<0.05	<0.05	<0.05
Total	97.61	95.88	96.92	96.58	97.34	94.07	92.5	96.27	97.06
Si	5.620	5.709	6.261	6.185	6.356	6.409	6.662	6.761	6.784
Al^{IV}	2.380	2.291	1.739	1.815	1.644	1.591	1.338	1.239	1.216
Al^{VI}	0.706	1.213	3.496	3.807	3.533	3.546	3.511	3.529	3.451
Ti	0.374	0.224	0.000	0.002	0.031	0.017	0.009	0.010	0.000
Fe	3.459	3.526	0.580	0.195	0.398	0.410	0.307	0.159	0.094
Mn	0.053	0.109	0.027	0.000	0.000	0.000	0.000	0.000	0.000
Mg	0.877	0.220	0.034	0.000	0.079	0.069	0.364	0.366	0.448
Ca	0.000	0.000	0.000	0.000	0.000	0.000	0.000	0.018	0.018
Na	0.051	0.024	0.042	0.094	0.023	0.013	0.000	0.033	0.023
K	1.893	1.992	1.921	1.868	1.932	1.902	1.392	1.490	1.712
Rb	0.000	0.019	0.000	0.000	0.000	0.000	0.000	0.000	0.000
Ba	0.000	0.000	0.000	0.000	0.000	0.000	0.000	0.000	0.000
OH	3.612	3.971	4.000	4.000	4.000	4.000	4.000	4.000	4.000
F	0.344	0.000	0.000	0.000	0.000	0.000	0.000	0.000	0.000
Cl	0.044	0.029	0.000	0.000	0.000	0.000	0.000	0.000	0.000
Z	8.000	8.000	8.000	8.000	8.000	8.000	8.000	8.000	8.000
Y	5.469	5.292	4.137	4.004	4.041	4.042	4.191	4.064	3.993
X	1.944	2.035	1.963	1.962	1.955	1.915	1.392	1.541	1.753
Fe/(Fe + Mg)	0.798	0.941	0.945	1.000	0.834	0.856	0.458	0.303	0.173

[a] Biotite situated in quartz

tion of xenotime (Fig. 6a). Energy-dispersive spectrometer analyses show that monazite which is partly altered to xenotime (close to the black arrow in Fig. 6a) is enriched in Th and Ca and depleted in LREE (cheralitic substitution). In strongly albitized episyenites monazite could not be observed any more. Magnetite is absent in all episyenites. HREE- and Th-bearing Nb–Ti–Y oxides are common early vug-filling minerals in strongly albitized episyenites (sample 97–10; Fig. 6b). Semi-quantitative EDS analyses of these Nb–Ti–Y oxides suggest they are polycrase-(Y) or aeschynite-(Y) as described by Hanson et al. (1992) in pegmatites. The general simplified formula can be written as $(Y,HREE,Th)(Ti,Nb)_2O_6$. Fluorite, fluocerite and ilmenite (or ilmenorutile) could not be found in episyenites.

Nearly euhedral pyrite occurs in some episyenites (Table 1). The relative age of pyrite formation is unclear. Vug-filling pyrite is often surrounded by chlorite and illite. For this reason, it could have been formed before or during the stage of chloritization and/or illitization. In sample 97–23 pyrite was altered to Fe hydroxides.

Whole-rock geochemistry

Königshain granites

Chemical analyses of unaltered Königshain granites, including some samples of reddened or moderately altered granites, are listed in Tables 4, 5, 6, and 7. The mean values of the equigranular and porphyritic granite types published by Eidam and Götze (1991) are given for comparison. Both the equigranular and porphyritic granites have a high SiO_2 content, but relatively low content of Fe_2O_3, MgO, TiO_2, and P_2O_5. They are very slightly peraluminous with A/CNK between 1.03 and 1.05 (only unaltered samples; Tables 4, 5). The equigranular granite differs from the porphyritic granite by higher Rb, HREE, and Y, and lower Fe_2O_3, MgO, TiO_2, Zr, Ba and LREE values (Figs. 7, 8; Tables 4, 5). The two granite types plot in separate fields in many chemical variation diagrams. They were formed by a multistage process of partial melting and sequential emplacement of fractional melts according to Eidam and Götze (1991).

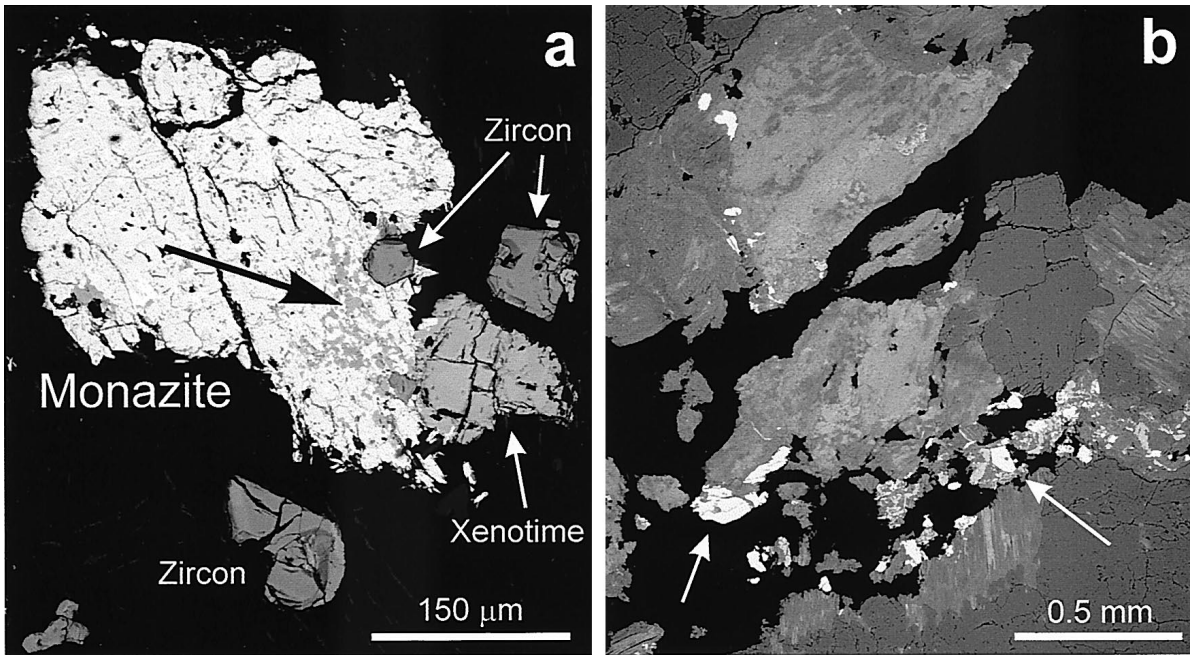

Fig. 6 **a** Backscattered electron image of porous monazite (*light gray*) which is altered to xenotime (*black arrow*), in moderately albitized equigranular granite (sample 97–19). **b** Backscattered electron image of HREE-bearing Nb–Ti–Y oxides (*white*) within or at the margin of vugs (*black*) in albitized episyenite (sample 97–10)

The equigranular granite is rich in SiO_2 (>77 wt.%), and low in Fe_2O_3 (1.12 wt.%), MgO (0.04 wt.%), CaO (0.46 wt.%) and TiO_2 (0.048 wt.%). Its low P_2O_5 content (<0.05 wt.%), its high content of Th (32–35 ppm), Y (52–61 ppm), Nb (28–30 ppm) and REEs (111 ppm) associated with a low peraluminous index (and low-Al biotite) are typical of highly fractionated low-P A-type granites (Pearce et al. 1984; Raimbault et al. 1991; Taylor 1992; Förster et al. 1995; Finger et al. 1997).

Episyenites

Chemical analyses of episyenites and altered granites with no quartz leaching are listed in Tables 5, 6, 7. The tunnel crosscuts the Königshain massif mainly within the equigranular granite type (see Fig. 2). Therefore, most of the episyenites investigated were formed by alteration of the equigranular granite except for sample 97–12 (Table 6). This is also evident from Zr/Th of episyenites which corresponds to the Zr/Th of the unaltered parent and is lower for the equigranular granite in comparison with the porphyritic granite (Fig. 7; Tables 4, 5, 6). The formation of episyenites and associated alterations have caused significant changes in chemical composition involving most major and trace elements. Figure 9 shows the analyses of the granites and episyenites plotted in the Q1-F1 diagram of Cathelineau (1986). Quartz leaching is demonstrated by a

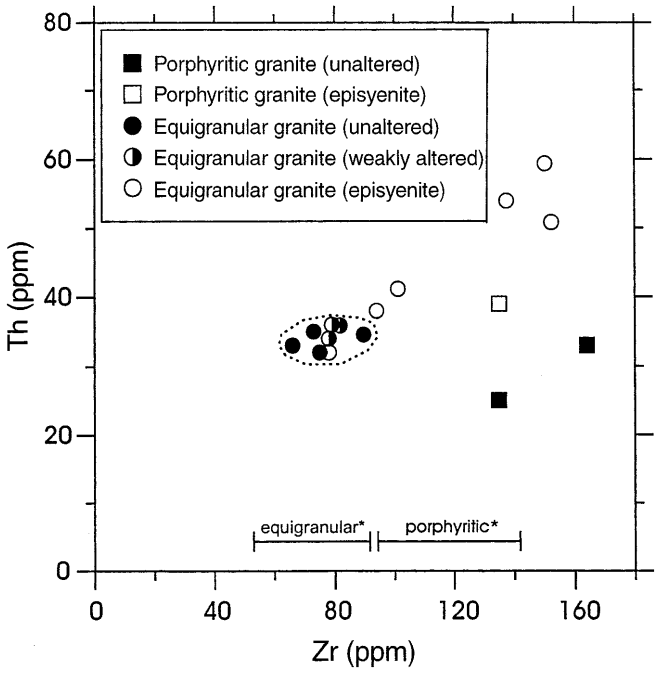

Fig. 7 Plot of Zr vs Th of unaltered granites and episyenites. *Asterisk* is range of Zr values of the porphyritic and equigranular granite according to Eidam and Götze (1991)

decrease of the Q1 parameter. In some episyenite samples the Q1 parameter is relatively high, however. Such values result from late filling of vugs by secondary idiomorphic quartz as can be seen in samples 97–11, 97–12, 97–23 and 97–29 (dashed arrows in Fig. 9). Part of the Q1 parameter increase can also result from feldspar dissolution or replacement by chlorite (sample 97–15). The F1 parameter allows to characterize the type of alkali metasomatism associated with episyenite

Table 4 Chemical composition of the porphyritic granite

Sample	18–14.7[a]	18–14.7[b]	13–13.1[c]	Eidam and Götze (1991)[d]
SiO_2 wt.%	74.44	75.57	75.19	–
Al_2O_3	13.62	13.51	13.60	13.38
Fe_2O_3 tot	1.44	1.28	1.17	1.54
MnO	0.020	0.039	0.023	0.031
MgO	0.21	0.22	0.15	0.22
CaO	1.04	1.12	0.76	1.01
Na_2O	3.82	3.63	3.70	3.66
K_2O	4.40	4.47	4.35	4.46
TiO_2	0.130	0.160	0.150	0.126
P_2O_5	<0.05	<0.04	<0.04	0.047
LOI	0.74	0.40	0.70	–
Total	99.9	100.5	99.8	–
As ppm	1.3	<20	<20	–
Ba	540	536	366	423
Be	6.4	n.a.	n.a.	7.3
Bi	0.1	n.a.	n.a.	–
Co	1.4	<8	<8	4.1
Cr	4.7	17.0	8.0	11
Cs	5.9	<30	<30	–
Cu	1.3	<8	<8	5
Ga	21	17	21	–
Ge	1.2	n.a.	n.a.	–
Hf	4.9	n.a.	n.a.	–
Mo	0.5	n.a.	n.a.	–
Nb	24	20	25	27
Ni	4	<6	<6	4
Pb	31.8	36.0	44.0	32
Rb	222	221	269	252
Sn	4.1	<30	<30	5.7
Sr	111.3	104	79	100
Ta	3.9	<20	<20	–
Th	25	26	33	–
U	13	<10	<10	–
V	6.1	6.0	<6	5.7
W	0.4	<30	<30	–
Y	28	27	29	37
Zn	25	27	33	–
Zr	135	135	164	120
A/CNK	1.05	1.05	1.12	1.05
N/NK	0.57	0.55	0.56	0.56
Zr/Hf	27.78	–	–	–

[a] ICP-AES and ICP-MS analysis
[b] XRF analysis
[c] Weak supergene alteration
[d] Mean values from this reference

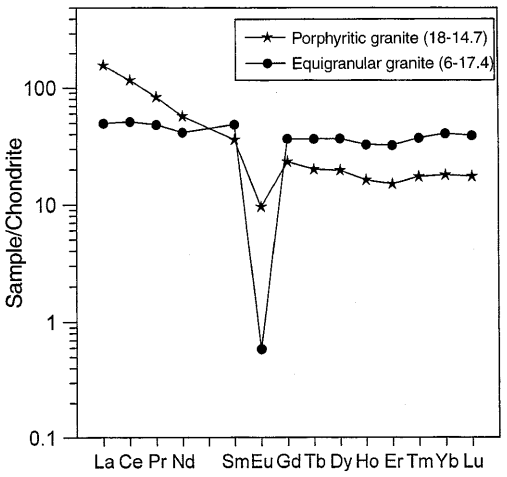

Fig. 8 Chondrite-normalized REE patterns of the equigranular and porphyritic granite

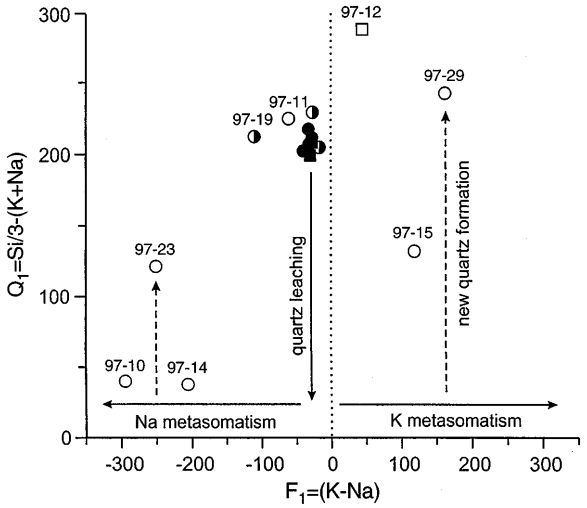

Fig. 9 Q1-F1 plot of granites and episyenites according to Cathelineau (1986). Note that the Q1 parameter may also increase due to alteration of feldspars (e.g. chloritization). For legend see Fig. 7

formation. Both Na and K metasomatism occur in episyenites. Samples with albitized feldspars are shifted towards a lower F1 parameter and may be classified as type-IIB episyenites according to Cathelineau (1986). Conversely, episyenites showing intensive illite alteration are shifted towards positive F1 values (Fig. 9). These samples resemble type-IV episyenites ("late retromorphoses") in the typology of Cathelineau (1986).

In order to avoid volume effects the "isocon" method of Grant (1986), which is based on work of Gresens (1967), was applied to estimate mass transfer. In all isocon plots of the Königshain episyenites Zr, Th, Hf and Ti show a coherent behaviour. These trace elements are considered to be almost immobile in the present case (see also Discussion). A volume loss of up to 40% during episyenite alteration has caused relative enrichment of Zr, Th, Hf and Ti, but did not significantly affect the ratios between these elements (e.g. Zr/Th in Fig. 7). The volume loss is due to quartz leaching which produces a vuggy rock. The vugs were not completely filled by authigenic minerals at later stages of hydrothermal activity. In addition, partial dissolution of feldspars can also account for some volume loss. A volume loss is even recognised in episyenites with a currently low porosity, because compaction of the porous rock combined with brecciation of the feldspar framework has strongly reduced the primary porosity. Mass transfer by hydrothermal fluids can only be suggested with some confidence if the deviation from

Table 5 Chemical composition of "unaltered" and moderately altered equigranular granite

Sample	"Unaltered"						Moderately altered		
	6–17.4[a]	6–17.4[b]	11–38–2[b]	9–41.5[b]	97–07[b]	Eidam and Götze (1991)[d]	97–38[b,c]	97–39[b,c]	97–19[b,e]
SiO_2 wt.%	77.15	77.80	77.61	77.50	77.48	–	77.63	76.35	77.02
Al_2O_3	12.57	12.30	12.68	12.30	12.67	14.06	12.07	12.82	13.56
Fe_2O_3 tot	0.92	0.78	0.88	0.72	0.88	1.12	0.81	1.32	0.64
MnO	0.020	0.022	0.032	0.019	0.035	0.025	0.084	0.010	<0.01
MgO	<0.05	<0.05	<0.05	<0.05	<0.05	0.04	<0.05	<0.05	0.09
CaO	0.32	0.42	0.41	0.41	0.45	0.46	0.16	0.23	0.06
Na_2O	4.16	3.94	3.86	3.84	3.99	3.89	3.58	3.69	5.08
K_2O	4.44	4.29	4.59	4.31	4.57	4.32	4.19	4.83	2.54
TiO_2	0.040	0.030	0.040	0.030	0.040	0.048	0.040	0.040	<0.01
P_2O_5	<0.05	<0.04	<0.04	<0.04	<0.04	0.015	<0.04	<0.04	<0.04
LOI	0.38	0.30	0.30	0.50	0.20	–	0.60	0.70	1.00
Total	100.0	99.8	100.4	99.5	100.4	–	99.2	100.0	100.0
As ppm	1.3	<20	<20	<20	<20	–	<20	<20	0.4
Ba	3	<20	<20	<20	<20	137	45	<20	22
Be	5.2	n.a.	n.a.	n.a.	n.a.	6.8	n.a.	n.a.	5.3
Bi	0.2	n.a.	n.a.	n.a.	n.a.	–	n.a.	n.a.	<0.04
Co	0.3	<8	<8	<8	<8	2.9	<8	<8	0.8
Cr	<4	<8	27.0	11.0	11.0	11	<8	<8	<8
Cs	8.0	<30	<30	<30	<30	–	<30	<30	3.6
Cu	1.7	<8	<8	<8	<8	2.2	<8	<8	0.8
Ga	22	20	20	21	24	–	17	20	23
Ge	1.4	n.a.	n.a.	n.a.	n.a.	–	n.a.	n.a.	1.2
Hf	5.6	n.a.	n.a.	n.a.	n.a.	–	n.a.	n.a.	4.7
Mo	0.6	n.a.	n.a.	n.a.	n.a.	–	n.a.	n.a.	0.1
Nb	30	29	28	28	29	36	27	35	34
Ni	<1.2	<6	<6	<6	<6	4	<6	<6	<1.2
Pb	43.6	47.0	48.0	97.0	48.0	42	35.0	38.0	2.9
Rb	332	361	350	345	348	351	301	377	224
Sn	8.7	<30	<30	<30	<30	6.6	<30	<30	12.5
Sr	1.5	<4	4	<4	<4	32	18	5	76.0
Ta	4.5	<20	<20	<20	<20	–	<20	<20	4.5
Th	35	32	35	33	32	–	36	34	36
U	12	<10	<10	13	12	–	<10	<10	15
V	<1.2	<6	<6	<6	<6	2	<6	<6	<1.2
W	2.3	<30	<30	<30	<30	–	<30	<30	2.8
Y	60	61	52	60	55	58	62	62	76
Zn	18	25	24	21	15	–	13	16	11
Zr	90	81	73	66	75	73	79	78	82
A/CNK	1.03	1.03	1.05	1.05	1.03	1.18	1.13	1.09	1.21
N/NK	0.59	0.58	0.56	0.58	0.57	0.58	0.56	0.54	0.75
Zr/Hf	16.09	–	–	–	–	–	–	–	17.34

[a] ICP-AES and ICP-MS analysis
[b] XRF analysis
[c] Sample with moderate sericitization and reddening
[d] Mean values from this reference
[e] Sample with moderate albitization of feldspars

the isocon is greater than primary variations of the unaltered parent and/or possible analytical bias. Thus, the mobility of elements that plot close to the isocon has to be interpreted with caution. The large scatter of the elements in the isocon plots of the Königshain episyenites suggest that most major and trace elements were mobilized to variable extent. Figures 10 and 11 show isocon plots of two episyenite types, one dominated by albitization with moderate chloritization (sample 97–10), and the other by chloritization and illitization (sample 97–15).

In albitized episyenites, albitization of feldspars has caused enrichment of Na and depletion of K, Ca, Ba, Rb, Cs and Pb (Fig. 10; Table 6). Albitized samples (97–10, 97–23, 97–14) are enriched in Sr, rather than depleted, as one would expect from albitization of the calcic part of plagioclase. The formation of typical Sr-bearing Ca minerals (e.g. fluorite, calcite, epidote) could not be identified in these samples. Strontium is likely to be enriched in newly formed hydrothermal albite as proposed by Schwartz and Surjono (1990) or Charoy and Pollard (1989). Strong mass transfer of REE is shown by the isocon plot (Fig. 10) and by the REE pattern (Fig. 12a) of sample 97–10. The LREE are depleted and the HREE (Gd to Lu) including Eu and Y are enriched. This general shift towards lower

Table 6 Chemical composition of episyenites

Sample Parent rock	97–10[a] Equigranular granite	97–11[b] Equigranular granite	97–14[a] Equigranular granite	97–15[a] Equigranular granite	97–23[a] Equigranular granite	97–29[b] Equigranular granite	97–12[b] Porphyritic granite
SiO_2 wt.%	61.80	66.50	58.32	45.01	72.04	73.19	65.40
Al_2O_3	19.81	16.12	21.06	24.08	16.56	14.10	15.36
Fe_2O_3 tot	3.42	3.95	4.95	11.68	1.19	2.03	6.98
MnO	<0.01	0.015	<0.01	0.050	<0.01	0.010	0.043
MgO	2.94	5.14	2.10	6.52	0.12	0.60	5.17
CaO	<0.05	<0.01	<0.05	<0.05	0.10	0.04	0.06
Na_2O	9.30	3.22	7.66	0.02	8.24	0.06	0.50
K_2O	0.27	2.03	1.96	5.64	0.72	7.75	2.86
TiO_2	0.04	0.04	0.03	0.07	0.03	0.03	0.10
P_2O_5	<0.05	<0.04	0.050	0.060	<0.05	<0.04	<0.04
LOI	2.41	3.30	3.86	6.11	1.03	2.00	3.90
Total	100.0	100.2	100.0	99.2	100.0	99.9	100.5
As ppm	0.6	<20	7.6	0.7	1.5	<20	<20
Ba	3	46	10	58	18	160	37
Be	4.9	n.a.	2.7	3.9	4.9	n.a.	n.a.
Bi	<0.04	n.a.	3.4	0.2	0.2	n.a.	n.a.
Co	0.4	8.0	36.0	12.7	0.6	16.0	<8
Cr	<4	17.0	<4	<4	<4	8.0	17.0
Cs	1.5	<30	2.9	3.0	1.3	<30	<30
Cu	0.7	<8	1.4	0.2	0.8	<8	<8
Ga	30	43	42	95	25	27	40
Ge	1.2	n.a.	0.8	1.4	0.9	n.a.	n.a.
Hf	10.0	n.a.	7.7	9.1	5.7	n.a.	n.a.
Mo	0.2	n.a.	114.9	0.3	0.7	n.a.	n.a.
Nb	57	30	54	34	63	35	24
Ni	6	<6	4	4	1	<6	<6
Pb	8.8	<10	57.2	3.5	3.5	78.0	<10
Rb	40	178	171	428	76	450	193
Sn	5.7	<30	10.9	23.6	7.3	<30	<30
Sr	17.2	12	16.2	1.3	85.1	6	<4
Ta	8.1	<20	5.5	4.8	11.1	<20	<20
Th	59	38	54	51	41	32	39
U	33	10	77	29	37	15	38
V	4.9	9.0	3.5	12.4	<1.2	<6	<6
W	2.6	<30	3.4	1.8	3.3	<30	<30
Y	232	67	122	75	134	111	55
Zn	21	26	16	49	8	15	42
Zr	150	94	138	152	101	78	135
A/CNK	1.27	2.15	1.43	3.92	1.14	1.65	3.81
N/NK	0.98	0.71	0.86	0.01	0.95	0.01	0.21
Zr/Hf	14.98	–	17.77	16.74	17.64	–	–

[a] ICP-AES and ICP-MS analysis
[b] XRF analysis

Table 7 REE analysis (ICP-MS) of granites and episyenites

Sample Rock type	18–14.7 Porphyritic granite	6–17.4 Equigranular granite	97–19 Equigranular granite	97–10 Episyenite	97–14 Episyenite	97–15 Episyenite	97–23 Episyenite
La (ppm)	38.29	12.14	3.60	2.24	4.52	13.30	6.08
Ce	74.10	32.71	7.82	4.76	6.04	6.01	21.44
Pr	8.02	4.65	1.87	1.26	2.76	4.93	2.56
Nd	27.17	19.63	10.44	8.05	15.37	21.94	12.69
Sm	5.53	7.47	5.58	7.87	10.30	8.62	7.83
Eu	0.56	0.03	0.07	1.21	0.52	0.42	0.62
Gd	4.74	7.44	6.96	17.28	12.94	8.83	11.67
Tb	0.75	1.36	1.46	4.36	2.79	1.68	2.51
Dy	4.97	9.30	10.04	35.95	20.98	11.54	17.66
Ho	0.92	1.85	2.37	8.17	4.59	2.50	4.11
Er	2.48	5.32	6.28	22.01	12.48	6.28	10.39
Tm	0.44	0.95	1.25	3.98	2.26	1.25	1.91
Yb	2.93	6.68	7.38	25.14	14.49	7.74	12.22
Lu	0.44	0.99	1.10	3.68	2.15	1.18	2.01

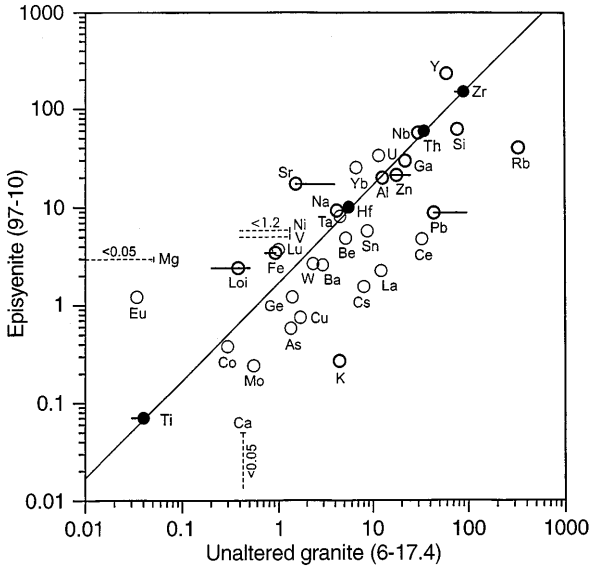

Fig. 10 Isocon plot of albitized episyenite (97–10) vs unaltered granite (6–17.4). Major elements in oxides (e.g. Na = Na_2O). For elements plotted in *bold circles* the compositional range of four unaltered samples (see Table 5) is indicated by a horizontal bar. The bar is only plotted if the compositional range is larger than the symbol. La + Ce and Yb + Lu are shown as representatives of LREE and HREE, respectively

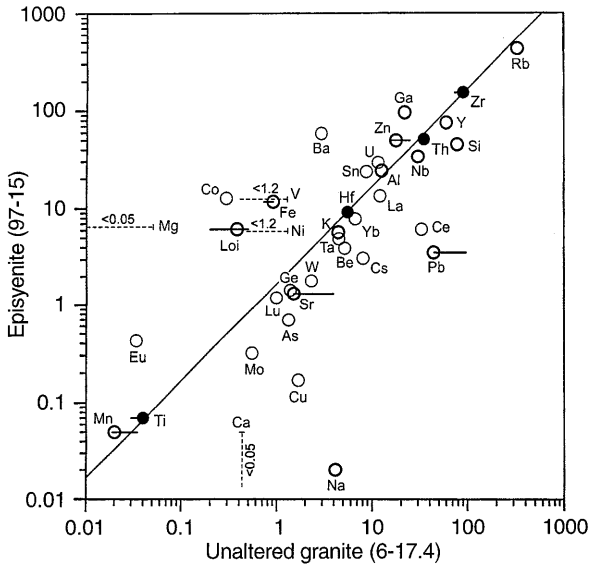

Fig. 11 Isocon plot of episyenite (97–15 with chloritization and illitization) vs unaltered granite (6–17.4). Major elements in oxides (e.g. Na = Na_2O). For elements plotted in *bold circles* the compositional range of four unaltered samples (see Table 5) is indicated by a *horizontal bar*. The bar is only plotted if the compositional range is larger than the symbol. La + Ce and Yb + Lu are shown as representatives of LREE and HREE, respectively

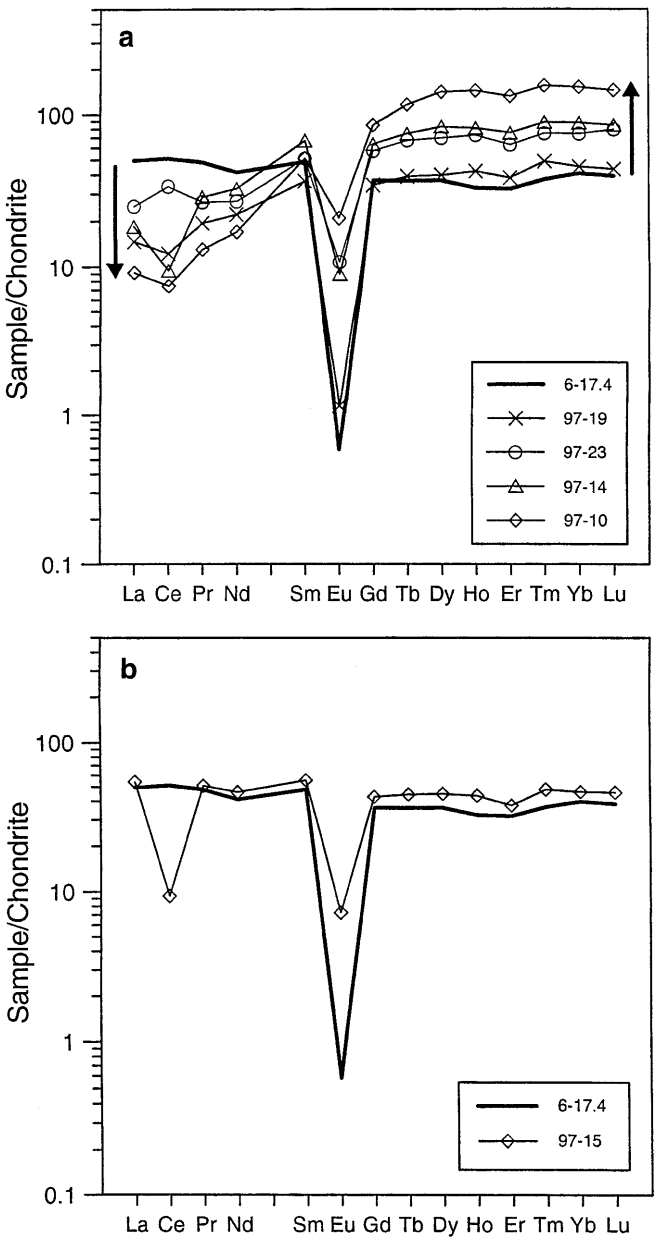

Fig. 12a,b Chondrite-normalized REE patterns of altered granites and episyenites in comparison with the unaltered equigranular granite (*bold line*). **a** Albitized episyenites including one sample of albitized granite (97–19, non episyenite). **b** Episyenite 97–15 with intensive chloritization and illitization

LREE/HREE is only observed in episyenites and granites that underwent albitization with molar $Na_2O/(Na_2O + K_2O) \geqslant 0.6$ (see N/NK in Tables 5, 6).

The chloritization of biotite can probably account for the depletion of As, Be, Cu, Mo, W, Sn and Zn. The enrichment of Mg, Fe, V, Ni and LOI (H_2O) is related to new formation of vug-filling chlorites. Increased values of Al, Ga and Co are likely to be associated with more intensive chloritization in sample 97–15 (Fig. 11).

The illitization of feldspars has led to the depletion of Ca, Na and Pb (Fig. 11). Depletion of Ce only occurs

in episyenites with enhanced illitization. This fact is most evident from episyenite 97–15 which displays a strong negative Ce anomaly, whereas the general chondrite-normalized pattern of all other REE is almost identical to that of the unaltered granite (Fig. 12b).

The episyenites with abundant vug-filling pyrite (97–14 and 97–29) are enriched in As, Bi, Co and Mo. All types of episyenites have enriched Eu values in comparison with the unaltered granite.

Discussion

Late-magmatic alteration

The equigranular granite shows late-magmatic alteration which pre-dates post-magmatic episyenitization. Late-magmatic alteration includes formation of secondary white mica (wm1), interstitial and replacive formation of fluorite and late growth of some monazite, fluocerite and ilmenite or ilmenorutile. These minerals are likely to crystallize at a late-magmatic stage. The fractionation of isovalent trace elements, such as REE and Zr–Hf in the equigranular granite, also support this interpretation. In silicate melt systems isovalent trace elements should be characterized by charge-and-radius-controlled (CHARAC) behaviour during magma fractionation (Bau 1996, and references therein). It ensues that element ratios of chemical twin pairs, such as Zr–Hf, should be close to chondritic values and REEs should display smooth normalized patterns. In the presence of fluids rich in strong complexing components (F, P, etc.) non-CHARAC trace element behaviour can result in fractionation of isovalent trace elements (Bau 1996). For example, non-CHARAC trace element behaviour is demonstrated by REE patterns that display the lanthanide tetrad effect which points to a subdivision of the REE into four concave-upward segments (Kawabe 1992; Bau 1996).

Non-CHARAC behaviour of some trace elements is clearly shown by the equigranular Königshain granite. The Zr/Hf of 16 (Table 5) is well below the CHARAC field ($26 < Zr/Hf < 46$) according to Bau (1996) and the REE pattern displays a slight but significant tetrad effect (Fig. 8). Such trace element behaviour as shown also by highly fractionated granites of the Fichtelgebirge was attributed to late-magmatic fractionation processes by deuteric fluids rich in strongly complexing agents such as F (Irber et al. 1997). In the equigranular Königshain granite fluorine may be responsible for the observed tetrad effect and Zr/Hf fractionation. Accessory fluorite indicates the presence of fluorine, although the average F content of the equigranular (829 ppm) granite is relatively low (data from Eidam and Götze 1991); however, fluorine could have been removed to some extent during the process of hydrothermal alteration. Evidence for fluorine mobilization is given by the F content of biotites in different textural position. Most biotite grains have access to the interstitial pore space and show a low fluorine content (< 0.6 wt.%; Table 3). Biotite grains enclosed in quartz, and therefore excluded from later hydrothermal alteration, have a higher F content of approximately 0.7 wt.%.

Post-magmatic hydrothermal alteration

The mineralogical and chemical data suggest at least two main stages of post-magmatic hydrothermal alteration including episyenitization. Stage 1 is characterized by albitization and quartz leaching. The relative age between albitization and quartz leaching is difficult to establish. Moderate albitization of feldspars also occurred within the granite outside the episyenite bodies; therefore, albitization is not restricted to episyenites and might have begun before quartz leaching. Authigenic albite and Nb–Ti–Y oxides grew first within vugs left by quartz leaching. The occurrence of Nb–Ti–Y oxides which are typical for pegmatite crystallization conditions (Cerny and Ercit 1989; Hanson et al. 1992) suggests the involvement of high-temperature late-magmatic fluids in alteration stage 1. In the course of granite cooling such fluids expelled from crystallizing granite could have been channelled along well defined structures (faults) in already solidified parts of the pluton, and in this way mixed with external fluids to produce episyenites. The mixing of magmatic and meteoric fluids during albitization including episyenitization in granites of the Emuford district, Australia, was proposed by Charoy and Pollard (1989). They emphasize a close genetic link between albitization and subsequent quartz-leaching and suggest that the exchange of Na for K in fluorine-rich hydrothermal fluids caused a substantial increase in quartz solubility and led to quartz dissolution in the albitized rock. Moreover, silica undersaturation can be due to drastic temperature changes in the range of 450–350 °C at pressures below 1 kb (Walter and Helgeson 1977; Fournier 1985). These conditions were confirmed by numerous fluid inclusion and/or stable isotope studies of many occurrence which indicate temperatures of episyenite formation to be commonly between 300 and 450 °C (Leroy 1978; Cathelineau 1986; Dempsey et al. 1990; Turpin et al. 1990; El Jarray et al. 1994; Recio et al. 1997). The condensation of vapours to low-salinity silica-undersaturated liquids at approximately 350 °C was also proposed to explain quartz dissolution (El Jarray et al. 1994). Low-pressure conditions, which facilitate post-magmatic quartz dissolution, are indicated by abundant miarolitic cavities in the equigranular granite.

Quartz-dissolution (stage 1) left a porous rock easily percolated by later hydrothermal fluids. During stage 2 the vugs were partly to completely filled by authigenic minerals such as chlorite, illite and quartz. There is petrographic and chemical evidence that chloritization and illitization were not preceded by albitization in

Table 8 Most significant mass transfer associated with main types of alteration in episyenites of the Köngshain massif. The same element can be mobilized during one or more alteration stages

	Depleted	Enriched
Quartz leaching	Si	
Albitization	Ca, K, Rb, LREE, Pb, Mo, As, Cu	Na, HREE, Y, Sr, U, Eu
Chloritization		Fe, Mg, V, Co, U, Ga, (Al), Loi (H_2O)
Illite alteration	Na, Ce ?	K, Rb, Ba, Eu ?, LOI (H_2O)
Pyrite formation		As, Bi, Co, Mo, (Fe, S)

some episyenites. Thus, quartz leaching outlasts albitization during stage 1 and locally produced non-albitized episyenites (Fig. 3d,e). In non-albitized episyenites K-feldspar and plagioclase were locally altered to illite during stage 2 (Fig. 3e), whereas previously albitized feldspars were almost unaffected by later illite alteration (Fig. 3f).

During post-magmatic hydrothermal alteration (stage 1 and 2) nearly all major and most trace elements have been mobilized due to dissolution or replacement of the main components and accessory minerals, and new formation of mineral phases. Since each episyenite sample generally represents a combination of two or more alteration phases (Table 1), depletion or enrichment of each individual element is not always related to one single type of alteration (Table 8). Nevertheless, the study of selected samples with one largely dominant alteration type enabled evaluation of specific mass transfers associated with each alteration event. Some trace elements, especially those which are usually referred to be immobile during hydrothermal alteration, show a complex behaviour.

Zirconium, Hf, Th and Ti are typical high field strength elements (HFSE) which are generally considered to be almost immobile during hydrothermal water–rock interaction. Experimental and natural evidences, however, have demonstrated that Zr, Ti and Th may be mobile especially in high-temperature (magmatic or hydrothermal) environments with strong complexing agents such as fluorine, sulphide and others (e.g. Gieré 1993; Keppler 1993; Rubin et al. 1993; Van Baalen 1993). Preliminary studies of accessory minerals in the granites of the study area indicate that zircon and monazite are the most important Zr- and/or Th-bearing minerals. Rubin et al. (1993) pointed out that Zr mobilisation by fluids is largely inhibited in the case of zircon being the major host of Zr, because of the high stability of this mineral. The lack of zircon corrosion or formation of authigenic Zr-bearing minerals in episyenites confirms the stability of Zr in these rocks. Monazite was altered in episyenite but newly formed Th-bearing polycrase-(Y) or aeschynite-(Y) had most probably incorporated the Th released by monazite alteration. This holds true also for Ti and Nb which were liberated by alteration of biotite, magnetite and probably ilmenite (or ilmenorutile) but fixed by newly formed accessory phases. Th, Ti and probably Nb and Ta were presumably mobilized locally within the hand specimen scale, but not significantly added or subtracted to larger rock volumes. The coherent enrichment of Zr, Hf, Th and Ti in episyenite samples in comparison with the unaltered parent (Figs. 10, 11) is consequently attributed to volume loss resulting mainly from quartz dissolution. For this reason these elements appeared to be most suitable for defining the isocon according to Grant (1986).

The REE content, especially that of albitized episyenites of Königshain, suggests significant REE mobility and fractionation during hydrothermal alteration (Fig. 10, 12). Similar to the HFSE discussed previously the REE are usually considered to be immobile during hydrothermal alteration by aqueous fluids. Nevertheless, REE mobility in the crust is largely controlled by the nature of their host minerals and composition of fluids involved in water–rock interaction (Humphries 1984). The REE may remain almost immobile during episyenite formation (Cathelineau 1987; Leroy and Turpin 1988; Dempsey et al. 1990; Hecht et al. 1994). If quartz dissolution is associated with alkali metasomatism, especially albitization, moderate to strong mobility and fractionation of REE is observed, however (e.g. Cathelineau 1987; Charoy and Pollard 1989; Petersson and Eliasson 1997). Among others, fluorine complexes are important for REE transport in hydrothermal fluids. The stability of fluorine complexes increases from the LREE towards the HREE (Wood 1990). In the present case complexing with fluorine could have caused the enrichment of HREE over LREE in hydrothermal fluids which then would have imprinted their REE pattern on albitized episyenites during water–rock interaction. Fluorine could derive from late-magmatic fluids or may have been mobilized from alteration of biotite and/or fluorite in the granite (see discussion on late-magmatic alteration). It is supposed that differential complexation of REE in the fluid, however, was not the primary reason for REE fractionation during hydrothermal alteration. The depletion of LREE is most likely to be related to the dissolution of monazite and possibly of other LREE-bearing minerals (e.g. fluocerite). Alteration of monazite was observed in the moderately albitized granite sample 97–19 (Fig. 6a). In strongly albitized episyenites (97–10) monazite is totally leached out. The HREE enrichment in albitized episyenites is explained by the formation of HREE-bearing Nb–Ti–Y oxide minerals of polycrase-(Y) or aeschynite-(Y) type. The same mineralogy has been described for albitized zones of a granitic pegmatite in the Truot Creek Pass District, Colorado, by Hanson et al. (1992). In the Königshain episyenites LREE depletion and HREE enrichment can develop to different extent and do not have to be exactly synchronous. For example, this is demonstrated

by the REE patterns of samples 97–19 and 97–23. Sample 97–23 is more enriched in HREE but less depleted in LREE in comparison with sample 97–19. These findings lead to the conclusion that REE fractionation during albitization of the Königshain granites and episyenites was essentially controlled by the breakdown or formation of accessory minerals in accordance with many other case studies (e.g. Cathelineau 1987; Hanson et al. 1992; Petersson and Eliasson 1997).

The Eu increase in episyenites (Figs. 10–12) suggests that the hydrothermal fluids displayed no negative or even a positive Eu anomaly. Enhanced Eu values (in relation to the other REE) in hydrothermal fluids can be a consequence of plagioclase breakdown (McLennan 1989). The desorption of divalent Eu from mineral surfaces during fluid migration at low oxygen fugacities (below the hematite/magnetite buffer) and at temperatures above 200–250 °C could be another reason for relative Eu enrichment in hydrothermal fluids (Bau 1991; Bau and Möller 1992). In any case deposition of Eu in the trivalent state together with other REEs in episyenites suggests oxidizing conditions during fluid–rock interaction.

Some episyenites with illite ± chlorite alteration display a negative Ce anomaly (Fig. 12). Ce^{3+} can be oxidized to Ce^{4+} and then fractionated from the other REE^{3+} during fluid–rock interaction. Möller and Bau (1993) argued that the development of a positive Ce anomaly in aerobic alkaline waters may be explained by the stabilization of (penta)carbonato-Ce^{IV}-complexes that hold Ce^{4+} in solution. The recrystallization of REE-bearing minerals under such conditions could explain the development of a negative Ce anomaly in episyenites. But this mechanism for Ce depletion cannot be directly related to the illitic alteration episodes, because such an alteration requires acidic fluids. The negative Ce anomaly of episyenites could be explained by hydrothermal recrystallization of REE-bearing minerals from a fluid which was previously depleted in Ce, e.g. by the formation of insoluble CeO_2 at oxidizing conditions. Thus, the negative Ce anomaly of episyenites suggests the circulation of external oxidizing fluids at stage 2. These fluids were most probably of meteoric origin.

Summary and conclusions

The following conclusions were reached as a result of this study:

1. Prior to episyenitization the equigranular granite of Königshain was affected by high-temperature late-magmatic alteration as indicated by non-CHARAC behaviour of some trace elements (REE with tetrad effect, Zr/Hf fractionation) and by late-stage formation or re-crystallization of accessory minerals (monazite, xenotime, fluorite).
2. Along well-defined structures the granites were exposed to intensive subsolidus hydrothermal alteration and in this way transformed to episyenites by selective leaching of magmatic quartz. The mineralogical and chemical data suggest at least two main stages of post-magmatic alteration. Stage 1 is characterized by albitization and/or subsequent quartz leaching including the formation of polycrase-(Y)- or aeschynite-(Y)-type minerals. Quartz leaching have also occurred without albitization resulting in the formation of non-albitized episyenites. During stage 2, feldspars of porous episyenites were altered to illite ± chlorite, and vugs were completely or partly filled by muscovite, quartz, pyrite, chlorite and illite. Illite and some quartz represent the latest vug-filling minerals in episyenites.
3. The new formation of polycrase-(Y) or aeschynite-(Y) in albitized episyenites suggests the involvement of high-temperature late-magmatic fluids. These low-salinity external fluids have mixed with the high-temperature late-magmatic fluids during episyenitization at stage 1. Quartz dissolution might be triggered by vapour condensation and/or cooling of low-salinity fluids below 450 °C along specific structures.
4. Almost all major and trace elements were enriched or depleted during one of the main alteration stages. Even typically immobile elements such as Th and Ti were mobile to some extent during recrystallization of accessory minerals, but not beyond the scale of the geochemical sample. Zirconium, Hf, Th and Ti were not involved in substantial mass transfer during hydrothermal alteration.
5. Albitized episyenites and granites show significant REE fractionation which results in a decreasing LREE content and increasing HREE content. It is concluded that mineralogical control, such as dissolution of monazite and/or new formation of HREE-rich polycrase-Y or aeschynite-Y and xenotime, essentially governed REE fractionation during albitization at stage 1. The development of negative Ce anomalies and enrichment of Eu is the only REE fractionation associated with illitization at stage 2. Such fractionation of Ce and Eu from the other REE requires oxidizing conditions during the final stage of post-magmatic alteration.

Acknowledgements We are grateful to M. Cathelineau (Nancy), P. Möller (Potsdam) and G. Spaun (Munich) for discussion, and M. Scholz (Munich) for field results and help. R. Beiderbeck (Munich) performed XRF analysis and S. Barda, R. Podor, and A. Kohler (Nancy) assisted with electron microprobe and SEM studies which is greatly acknowledged. The manuscript benefited from comments and suggestions by M. Bau, M. Engi and P. Nabelek.

References

Bau M (1991) Rare-earth element mobility during hydrothermal and metamorphic fluid–rock interaction and the significance of the oxidation state of europium. Chem Geol 93:219–230

Bau M (1996) Controls of the fractionation of isovalent trace elements in magmatic and aqueous systems: evidence from Y/Ho, Zr/Hf, and lanthanides tetrad effect. Contrib Mineral Petrol 123:323–333

Bau M, Möller P (1992) Rare earth element fractionation in metamorphogenic hydrothermal calcite, magnesite and siderite. Mineral Petrol 45:231–246

Cathelineau M (1986) The hydrothermal alkali metasomatism effects on granitic rocks: quartz dissolution and related subsolidus changes. J Petrol 27:945–965

Cathelineau M (1987) U–Th–REE mobility during the albitization and quartz dissolution in granitoids: evidence from southeast French Massif Central. Bull Minéral 110:249–259

Cerny P, Ercit TS (1989) Mineralogy of niobium and tantalum: crystal chemical relationships, paragenetic aspects and their economic implications. In: Möller P, Cerny P, Saupé F (eds) Lanthanides, tantalum and niobium. Springer, Berlin Heidelberg New York, pp 27–79

Charoy B, Pollard PJ (1989) Albite-rich, silica-depleted metasomatic rocks at Emuford, Northeast Queensland: mineralogical, geochemical and fluid inclusion constraints on hydrothermal evolution and tin mineralization. Econ Geol 84:1850–1874

Cheilletz A, Giuliani G (1982) Role de la déformation du granite dans la genèse des épisyenites feldspathiques des massifs de Lovios-Geres (Galice) et des Zaer (Maroc Central). Mineral Deposita 17:387–400

Dempsey CS, Meighan IG, Fallick AE (1990) Desilication of Caledonian granites in the Barnesmore complex, Co. Donegal: the origin and significance of metasomatic syenite bodies. J Geol 25:371–380

Dill H (1985) Die Vererzung am Westrand der Böhmischen Masse – Metallogenese in einer ensialischen Orogenzone. Geologisches Jahrbuch, D 73. Bundesanstalt für Geowissenschaften und Rohstoffe, Hannover

Eidam J, Götze J (1991) The granitic massif of Königshain-Arnsdorf (Lusatian Anticlinal Zone): an example of a reversely zoned pluton. Chem Erde 51:55–71

Eidam J, Hammer J, Korich D, Bielicki K-H (1995) Amphibole-baring granites in the Lusatian Anticlinal Zone: Variscan I-type magmatism at the northern margin of the Bohemian Massif. N Jahrb Mineral Abh 168:259–281

El Jarray A, Boiron M-C, Cathelineau M (1994) Percolation microfissurale de vapeurs aqueuses dans le granite de Pény (Massif de Saint Sylvestre, Massif Central): relation avec la dissolution du quartz. CR Acad Sci Paris 318:1095–1102

Finger F, Roberts MP, Haunschmid B, Schermaier A, Steyrer HP (1997) Variscan granitoids of central Europe: their typology, potential sources and tectonothermal relations. Mineral Petrol 61:67–96

Förster H-J, Seltmann R, Tischendorf G (1995) High-fluorine, low-phosphorous A-type (postcollision) silicic magmatism in the Erzgebirge. Terra Nostra 7/95:32–35

Fournier RO (1985) The behavior of silica in hydrothermal solutions. In: Berger BR, Bethke PM (eds) Geology and geochemistry of epithermal systems. Soc Econ Geol Rev Econ Geol 2:45–61

Gieré R (1993) Transport and deposition of REE in H_2S-rich fluids: evidence from accessory mineral assemblages. Chem Geol 110:251–268

Govindaraju K, Mévelle G (1987) Fully automated dissolution and separation methods for ICP rocks analysis. Application to the determination of rare earth elements. J Anal At Spectrom 2:615–621

Govindaraju K, Mévelle G, Chouard C (1976) Automated optical emission spectochemical bulk analysis of silicate rocks with microwave plasma excitation. Anal Chem 48:1325–1331

Grant JA (1986) The isocon diagram: a simple solution to Gresens equations for metasomatic alteration. Econ Geol 81:1976–1982

Gresens RL (1967) Composition-volume relationships of metasomatism. Chem Geol 2:47–65

Hanson SL, Simmons WB, Webber KL, Falster AU (1992) Rare-earth-element mineralogy of granitic pegmatites in the Trout Creek Pass district, Chaffee County, Colorado. Can Mineral 30:673–686

Hecht L, Spiegel W, Morteani G (1991) Multiphase alteration including disseminated uranium mineralization in quartz-depleted granites (episyenites) of the Fichtelgebirge (northeastern Bavaria, Germany). In: Pagel M, Leroy L (eds) Source, transport and deposition of metals. Balkema, Rotterdam, pp 53–56

Hecht L, Spiegel W, Morteani G (1994) Geochemistry and petrography of unaltered granites and their host rocks: Fichtelgebirge granites. In: Haslam HW, Plant JA (eds) Granites, metallogeny, lineaments and rock–fluid interactions: a study of granites and associated rocks in the French and German Hercynides and the British Caledonides. BGS Research Report. British Geological Survey, Keyworth, pp 143–177

Humphries SE (1984) The mobility of the rare earth elements in the crust. In: Henderson P (ed) Rare earth element geochemistry. Elsevier, Amsterdam, pp 315–341

Irber W, Förster HJ, Hecht L, Möller P, Morteani G (1997) Experimental, geochemical, mineralogical and O-isotope constraints on the late-magmatic history of the Fichtelgebirge granites (Germany). Geol Rundsch 86:S110–S124

Kawabe I (1992) Lanthanide tetrad effect in the Ln^{3+} ionic radii and refined spin-pairing energy theory. Geochem J 26:309–335

Keppler H (1993) Influence of fluorine on the enrichment of high field strength trace elements in granitic rocks. Contrib Mineral Petrol 114:479–488

Krauss M, Eidam J, Hammer J, Korich D (1992) Die cadomisch-variszische Entwicklung des Lausitzer Granodiorit-Komplexes. Zbl Geol Paläontol Teil I 1/2:71–85

Kröner A, Hegner E, Hammer J, Haase G, Bielicki K-H, Krauss M, Eidam J (1994) Geochronology and Nd–Sr systematics of Lusatian granitoids: significance for the evolution of the Variscan orogen in east-central Europe. Geol Rundsch 83:357–376

Lacroix MA (1920) Les roches éruptives du Crétace pyrénéen et la nomenclature des roches éruptives modifiées. Comptes Rendues Acad Sci France 170:685–690

Leroy J (1978) The Fany and Margnac uranium deposits of the La Crouzilee district (Western Massif Central, France): geologic and fluid inclusion studies. Econ Geol 73:1611–1634

Leroy JL, Turpin L (1988) REE, Th and U behaviour during hydrothermal and supergene processes in a granitic environment. Chem Geol 68:239–251

McLennan SM (1989) Rare earth elements in sedimentary rocks: influence of provenance and sedimentary processes. In: Lipin BR, McKay GA (eds) Geochemistry and mineralogy of rare earth elements. Rev Mineral, pp 1209–1264

Möbus G, Lindert W (1967) Das Granitmassiv von Königshain bei Görlitz (Oberlausitz). Abh Dtsch Akad Wissenschaft Kl Bergbau Hüttenwesen Montangeol 1:81–160

Möller P, Bau M (1993) Rare-earth patterns with positive cerium anomaly in alkaline waters from Lake Van, Turkey. Earth Planet Sci Lett 117:671–676

Pearce JA, Harris NBW, Tindle AG (1984) Trace element discrimination diagrams for tectonic interpreation of granitic rocks. J Petrol 25:956–983

Petersson J, Eliasson T (1997) Mineral evolution and element mobility during episyenitization (dequartzification) and albitization in the postkinematic Bohus granite, southwest Sweden. Lithos 42:123–146

Raimbault L, Charoy B, Cuney M, Pollard PJ (1991) Comparative geochemistry of Ta-bearing granites. In: Pagel M, Leroy L (eds) Source, transport and deposition of metals. Balkema, Rotterdam, pp 793–796

Recio C, Fallick AE, Ugidos JM, Stephens WE (1997) Characterization of multiple fluid-granite interaction processes in the episyenite of Avila-Béjar, Central Iberian Massif, Spain. Chem Geol 143:127–144

Rubin JN, Henry CD, Price JG (1993) The mobility of zirconium and other "immobile" elements during hydrothermal alteration. Chem Geol 110:29–47

Scaillet S, Cuney M, Le Carlier de Veslud C, Cheilletz A, Royer JJ (1996) Cooling pattern and mineralization of the Saint Syvestre and Western Marche leucogranite pluton, French Massif Central: II. Thermal modelling and implications for the mechanism of uranium mineralization. Geochim Cosmochim Acta 60:4673–4688

Schoch AE, Scheepers R (1990) The distribution of uranium and thorium in the Cape Columbine granite from the Southwestern Cape Province, South Africa. Ore Geol Rev 5:223–246

Schwartz MO, Surjono (1990) Greisenization and albitization at the Tikus Tin-Tungsten deposit, Belitung, Indonesia. Econ Geol 85:691–713

Slaby E (1992) Changes in the structural state of secondary albite during progressive albitization. N Jahrb Miner Mh 7:321–335

Taylor RP (1992) Petrological and geochemical characteristics of the pleasant ridge Zinnwaldite-Topaz granite, southern New Brunswick, and comparison with other Topaz-bearing felsic rocks. Can Mineral 30:895–921

Turpin L, Leroy JL, Sheppard SMF (1990) Isotopic systematics (O, H, C, Sr, Nd) of superimposed barren and U-bearing hydrothermal systems in a Hercynian granite, Massif Central, France. Chem Geol 88:85–98

Van Baalen MR (1993) Titanium mobility in metamorphic systems: a review. Chem Geol 110:233–249

Walter JV, Helgeson HC (1977) Calculation of the thermodynamic properties of aqueous silica and the solubility of quartz and its polymorph at high temperatures and pressures. Am J Sci 277:1315–1351

Wood SA (1990) The aqueous geochemistry of the rare-earth elements and yttrium, 2. Theoretical predictions of speciation in hydrothermal solutions to 350 °C at saturation water vapor pressure. Chem Geol 88:99–125